11

Generation and Detection of Mesoscopic Pulsed States of Light for Quantum Information

Alessia Allevi[1] and Maria Bondani[2]
[1]*Dipartimento di Fisica e Matematica - Università degli Studi dell'Insubria*
U.d.R. Como - Consorzio Nazionale Interuniversitario per le Scienze fisiche della Materia
[2]*Istituto di Fotonica e Nanotecnologie - Consiglio Nazionale delle Ricerche*
U.d.R. Como - Consorzio Nazionale Interuniversitario per le Scienze fisiche della Materia
Italy

1. Introduction

Generation and measurement of quantum states of the electromagnetic field represent a hot and widely discussed topic in the Physics community, since optical states are useful not only in fundamental experiments but also in several applications in the fields of Quantum Optics and Quantum Information (Bouwmeester et al., 2000). In fact, optical radiation is endowed with relevant characteristics as it travels at maximum possible speed, it is almost unaffected by the interaction with the environment, which in many cases represents an unavoidable decoherence source, and it can be integrated in optoelectronic circuits to implement quantum computing protocols (Sansoni et al., 2010). The possibility of using optical fields in applicative protocols depends on the capability of generating and manipulating optical states that are robust with respect to losses (i.e. that contain a sizeable number of photons) and that can be produced and measured at high rate. For all these reasons, mesoscopic pulsed optical states containing few tens of photons per pulse seem to be the ideal candidates for applications to quantum communication protocols in which each pulse must be addressed individually. Moreover, the problem of generating suitable pulsed states must be considered together with the question of their measurement and characterization. In fact, nowadays we have many types of pulsed-light sources at our disposal, each of them characterized by different pulse durations (from few fs up to few ns), different pulse-repetition rates (from few Hz to 100 MHz) and a wide range of energies per pulse (from few nJ to several J). However, not all these pulsed light can be easily measured. In the mesoscopic intensity regime, for example, detectors endowed with photon-number resolution are required so as to determine shot-by-shot photon numbers or, at least, to characterize some features of the optical states. In fact, full characterization of the optical state, obtained *e.g.* by evaluating its Wigner function, can be achieved with optical homodyne tomography (OHT) (Raymer, 1997), a technique that over the years has proved its effectiveness in reconstructing both classical and quantum states, even if further optimizations are needed in the case of pulsed fields (Zavatta et al., 2006).
Direct detection schemes are an alternative to OHT in all the cases in which knowing the statistics of detected photons is sufficient to characterize the signal state, as demonstrated in the pioneering work of Arecchi (Arecchi, 1965). Obviously, the implementation of a direct detection scheme requires a proper choice of the detector, the development of a calibration

strategy and a robust reconstruction method independent of any a-priori knowledge of the state under investigation. For example, valuable results have been obtained by means of an ON/OFF method assisted by a maximum likelihood algorithm (Zambra et al., 2005).
To this aim, several different strategies are being followed either to improve the traditional detectors or to build new ones (Haderka et al., 2010). In fact, the mature silicon-based technologies have encouraged the optimization of both photomultipliers and avalanche photodiodes, by enhancing their quantum efficiency (*QE*) and reducing their dark-count rate. More recently, a new type of detector, usually called hybrid photodetector (HPD), as it combines a photocathode with a diode structure operated below the breakdown threshold, has been developed and successfully tested (Bondani et al., 2009a). As in this case the amplification process takes part in one step, the excess noise is small enough to allow photon-number resolution (up to 6 detected photons). The *QE*, mainly given by the photocathode, can reach good values (up to 0.5 in the visible range), whereas the dark-count rate can be neglected. As an alternative, the accomplishment of photon-counting capability can be obtained by splitting the light to be measured either in space or in time prior to detection so that at most one photon at a time hits the detector sensitive area. Among them, we mention the visible light photon counter (VLPC) (Kim et al., 1999); the fiber-loop detector, which is a time-multiplexed detector based on one (Rehacek et al., 2003) or more (Fitch et al., 2003) single-photon avalanche diodes (SPADs); the Silicon photomultiplier (SiPM), that is constituted by a matrix of SPADs with a common output (Akindinov et al., 1997). Due to their composite structure, SiPMs have a good photon-counting capability, though presenting large dark-count rate (600 kHz) and cross-talk probability (Afek et al., 2009; Ramilli et al., 2010). Finally, two types of CCD cameras can be used to detect light in the mesoscopic domain, namely the intensified CCD (iCCD) (Haderka et al., 2005) and the electron-multiplied CCD (EM-CCD) (Blanchet et al., 2008).
In the last decade, a tremendous progress has been achieved in the field of superconductors so that new types of detectors have been developed, such as the transition-edge sensor (TES) (Lita et al., 2008) and the superconducting nanowires (Gol'tsman et al., 2001). Despite having a good *QE*, these detectors must operate at cryogenic temperatures and thus they are rather cumbersome. As of today, the ideal detector has yet to appear and the optimal choice is application specific.

2. Theory

We present the procedure for analyzing the output of a detector measuring light pulses in order to recover light statistics (Andreoni & Bondani, 2009a). With reference to Fig. 1, we consider a pulsed light field having photon-number distribution, P_n. The field is delivered to the detector by suitable optics and the overall losses of the detection chain are summarized by a single factor η, which represents the overall photon-detection efficiency of the apparatus. Since $\eta < 1$, the distribution of the number of detected photons, P_m, and the photon-number

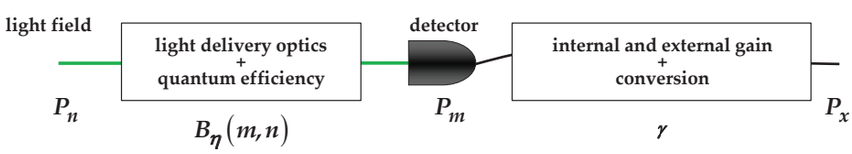

Fig. 1. Scheme for light detection: η is the overall detection efficiency and γ is the overall gain.

distribution P_n are linked by

$$P_m = \sum_{n=m}^{+\infty} B_\eta(m,n) P_n = \sum_{n=m}^{+\infty} \binom{n}{m} \eta^m (1-\eta)^{n-m} P_n \,, \tag{1}$$

from which we obtain the relation between the first moments of photons and detected-photon distributions: $\langle m \rangle = \eta \langle n \rangle$, $\langle m^2 \rangle = \eta^2 \langle n^2 \rangle + \eta(1-\eta)\langle n \rangle$ (Bondani et al., 2009a).
We consider a detector operated within its range of linearity on pulsed light states. The output pulses of the detector are amplified and integrated (see Fig. 1) over a time-gate synchronous with the detector output pulse and slightly longer than its time duration (typically few nanoseconds). The output of the integrator is then sampled and digitized. The final output number x is stored in the memory of a computer to be processed offline. The obtained pulse-height spectrum normalized to its integral can be interpreted as the probability density P_x of the variable x. The zero of the x-scale is set at the value that is equal to the mean of the experimental P_x distribution obtained in the absence of light. The overall conversion process of the m detected photons into a x-value can be characterized by a single conversion factor γ, which is a stochastic variable distributed according to p_γ and having mean value $\overline{\gamma}$ and variance σ^2.
As the detection events giving different m values are mutually exclusive, P_x can be written as

$$P_x = P_{m=0} p_\gamma^{(0)} + P_{m=1} p_\gamma + P_{m=2}(p_\gamma * p_\gamma) + \ldots + P_{m=k}(p_\gamma * p_\gamma * \ldots * p_\gamma)_k \,, \tag{2}$$

where $p_\gamma^{(0)}$ is the probability density of the x values in the absence of light, whose mean value is zero by definition, and the $*$ symbols indicate convolution products. Note that we allow $p_\gamma^{(0)}$ to be different from p_γ, which accounts for the fact that in photoemissive detectors the anodic charge distribution for dark counts is different from that of the single-electron response (SER). The output values $x^{(k)}$ recorded when k photons are detected is given by $x^{(k)} = \sum_{i=1}^{k} \gamma_i$ where all γ_i are distributed according to p_γ. We can thus write for the cumulants (Mandel & Wolf, 1995) $\kappa_r^{(\sum_{i=1}^{k} \gamma_i)} = \sum_{i=1}^{k} \kappa_r^{(\gamma_i)}$, in which $\kappa_1^{(\gamma_i)} = \overline{\gamma}$, $\kappa_2^{(\gamma_i)} = \sigma^2$, $\kappa_3^{(\gamma_i)} = \widetilde{\mu}_3$, $\kappa_4^{(\gamma_i)} = \widetilde{\mu}_4 - 3\sigma^4$, $\kappa_5^{(\gamma_i)} = \widetilde{\mu}_5 - 10\sigma^2\widetilde{\mu}_3$ and $\widetilde{\mu}_r$ are the values assumed for the central moments of p_γ. In the case of $r = 1$ we get

$$\langle x \rangle = \overline{\gamma} \sum_{k=0}^{+\infty} k P_{m=k} = \langle m \rangle \overline{\gamma} \,. \tag{3}$$

We can now relate the central moments $\mu_r(x) = \langle (x - \langle x \rangle)^r \rangle$ of the experimental P_x to those of the unknown probability density P_m, $\mu_r(m) = \langle (m - \langle m \rangle)^r \rangle$

$$\mu_r(x) = \sum_{k=0}^{+\infty} P_{m=k} \int_{-\infty}^{+\infty} (x - \langle x \rangle)^r (p_\gamma * p_\gamma * \ldots * p_\gamma)_k dx \; = \sum_{k=0}^{+\infty} P_{m=k} \mu_r(x^{(k)}) \,, \tag{4}$$

where $\mu_r(x^{(k)}) \equiv \int_{-\infty}^{+\infty} (x - \langle x \rangle)^r (p_\gamma * p_\gamma * \ldots * p_\gamma)_k dx$. For $r = 1$ Equation 4 obviously vanishes. For $r \geq 2$ we insert the binomial expansion $(x - \langle x \rangle)^r = \sum_{j=0}^{r} \binom{r}{j} x^j (-\langle x \rangle)^{r-j}$ and use Equation 3 to find

$$\mu_r(x) = \sum_{j=0}^{r} \binom{r}{j} (-\langle m \rangle \overline{\gamma})^{r-j} \sum_{k=0}^{+\infty} P_{m=k} \mu'_j(x^{(k)}) \,, \tag{5}$$

in which the "prime" distinguishes the moments from the central moments. It can be shown (Andreoni & Bondani, 2009a) that the moments $\mu'_j(x^{(k)})$ are polynomials whose terms contain the number of detected photons and the cumulants of the probability distribution p_γ. The results for $r = 2$ and $r = 3$ are

$$\frac{\mu_2(x)}{\langle x\rangle} = \overline{\gamma}\left(\frac{\mu_2(m)}{\langle m\rangle} + \frac{\sigma^2}{\bar{\gamma}^2}\right) \tag{6}$$

$$\frac{\mu_3(x)}{\langle x\rangle} = \overline{\gamma}^2\left(\frac{\mu_3(m)}{\langle m\rangle} + 3\frac{\mu_2(m)}{\langle m\rangle}\frac{\sigma^2}{\bar{\gamma}^2} + \frac{\tilde{\mu}_3}{\bar{\gamma}^3}\right). \tag{7}$$

If p_γ is narrow enough so that $\sigma^2/\overline{\gamma}^2 \to 0$ only one term of the polynomials survives and $\mu'_j(x^{(k)})$ reduces to $\mu'_j(x^{(k)}) \cong k^j(\kappa_1^{(\gamma_i)})^j = k^j\overline{\gamma}^j$, which we substitute into Equation 5 to obtain $\mu_r(x) = \overline{\gamma}^r\mu_r(m)$ (Andreoni & Bondani, 2009a) that we conveniently rewrite as

$$\frac{\mu_r(x)}{\langle x\rangle} = \overline{\gamma}^{r-1}\frac{\mu_r(m)}{\langle m\rangle}. \tag{8}$$

The link between $\mu_r(x)$ and $\mu_r(m)$ in Equation 8, which holds when σ is sufficiently smaller than $\overline{\gamma}$, shows that the simple knowledge of $\overline{\gamma}$ allows retrieving P_m from P_x, since Equation 8 holds for moments of any order and guarantees that the distribution that is obtained by binning the values x data into bins of width $\overline{\gamma}$ coincides with P_m.
The result in Equation 8 allows adopting a self-consisting procedure to determine $\overline{\gamma}$ without calibrating both detector and signal processing electronics, but simply using the measurements performed to determine P_x for the light field under investigation and without any previous knowledge of its statistics (Bondani et al., 2009a;b;c). In fact, by taking into account the properties derived from Equation 1, we can calculate

$$F_m \equiv \frac{\mu_2(m)}{\langle m\rangle} = \frac{\eta^2\mu_2(n) + \eta(1-\eta)\langle n\rangle}{\eta\langle n\rangle} = \eta F_n + 1 - \eta = \eta Q + 1, \tag{9}$$

in which $F_n = \mu_2(n)/\langle n\rangle$ is the Fano factor and $Q = (\mu_2(n) - \langle n\rangle)/\langle n\rangle$ is the Mandel parameter of the light entering the experimental apparatus in Fig. 1 and containing $\langle n\rangle$ photons in the measure time T_M (Mandel & Wolf, 1995). In analogy to light, we define a sort of Fano factor for detected photons, $F_m = \mu_2(m)/\langle m\rangle$, and for outputs, $F_x = \mu_2(x)/\langle x\rangle$. Substituting Equation 9 into Equation 8 with $r = 2$ and using Equation 3 yields

$$F_x = \frac{\mu_2(x)}{\langle x\rangle} = \frac{Q}{\langle n\rangle}\langle x\rangle + \overline{\gamma}\left(1 + \frac{\sigma^2}{\overline{\gamma}^2}\right). \tag{10}$$

Equation 10 is the key result of our method that allows determining $\overline{\gamma}$ by a self-consistent procedure when $\sigma^2/\overline{\gamma}^2 \ll 1$, that is when Equation 8 holds. In fact, since measurements performed on the same input light with different η-values, thus producing different $\langle x\rangle$-values, would leave the factor $Q/\langle n\rangle$ unaltered, the plots of F_x as a function of $\langle x\rangle$ should exhibit a linear dependence with slope $Q/\langle n\rangle$ with $\overline{\gamma}$ as the intercept. The value of the slope is significant of the statistics of the number of photons P_n, being it zero for coherent light, positive for light with super-poissonian variance and negative for light with sub-poissonian variance (Mandel & Wolf, 1995). In the following Sections we will show the retrieval of the slope values for several different light states (Bondani et al., 2009a;b;c).

3. Validation of the theory

We tested the analysis method by measuring a coherent light with a number of linear detectors endowed with different features. In all the measurements presented here, the coherent light was provided by the second-harmonic output of a Nd:YLF mode-locked laser amplified at 5 kHz (High Q Laser Production, Austria) producing pulses of ∼5.4 ps duration at 523 nm wavelength. To minimize the collection of stray light, we used a multimode fiber to deliver the light to the detectors. Unless otherwise indicated, the output current pulses of the detectors were suitably gate-integrated by SR250 modules (Stanford Research Systems, CA) over integration gates shorter than 500 ns and sampled to produce a voltage which was digitized and recorded at each shot to produce the output x. The variation of η required to implement the analysis was obtained by inserting a variable neutral-density filter or a polarizer in the beam path. The linearity of the detectors allows the determination of the actual value of η.
For a coherent field we expect a Poissonian photon-number distribution

$$P_n = \frac{\langle n \rangle^n}{n!} \exp(-\langle n \rangle) \,, \tag{11}$$

for which mean value and variance are $\langle n \rangle$ and $Q = 0$. By applying Equation 1 to Equation 11 we obtain $P_m = \langle m \rangle^m / m! \exp(-\langle m \rangle)$, that has mean value $\langle m \rangle = \eta \langle n \rangle$, which means that the statistics is still Poissonian. We remark that this property of invariance of the statistical distribution under Bernoullian convolution has a more general application and holds in particular for all the states considered in this Chapter. For a coherent light we have

$$F_x = \frac{\mu_2(x)}{\langle x \rangle} = \overline{\gamma} \,, \tag{12}$$

independent of the mean value $\langle x \rangle$. The value of $\overline{\gamma}$ obtained from the experimental values of F_x is then used to convert the output x into a number of detected photons m and to re-bin the data to obtain the experimental probability distribution of detected photons $P_{m,\mathrm{exp}}$. The quality of the reconstructed distributions can be estimated by their fidelity f with the expected theoretical distributions P_m (Jozsa, 1994)

$$f = \sum_{m=1}^{\infty} \sqrt{P_{m,\mathrm{exp}} P_m} \,. \tag{13}$$

3.1 Photon-resolving photomultiplier

The first detector we tested is the Quantacon Burle 8850 photomultiplier ($\mathrm{PMT_{Burle}}$, Burle Industries Inc.). This photomultiplier is based on a semitransparent bialkali photocathode (maximum $QE = 0.24$ at ∼400 nm) and a first dynode with a high-gain followed by 11 dynodes. The $\mathrm{PMT_{Burle}}$ detector is endowed with partial photon resolving capability, *i.e.* it gives partially distinct outputs for different numbers of photons detected within the pulse-response time-duration. The detector has 200 counts/s of dark noise, that give a negligible contribution in the gate time. The after-pulse probability has no effect on the detection since the light source is operated at 500 Hz. In Fig. 2(*a*) we show some typical pulse-height spectra of the $\mathrm{PMT_{Burle}}$ at different light intensities. We note that the pulse-height spectra lose the peak structure as soon as the field intensity becomes mesoscopic but remain linear in the mean values over a wide range of intensities.

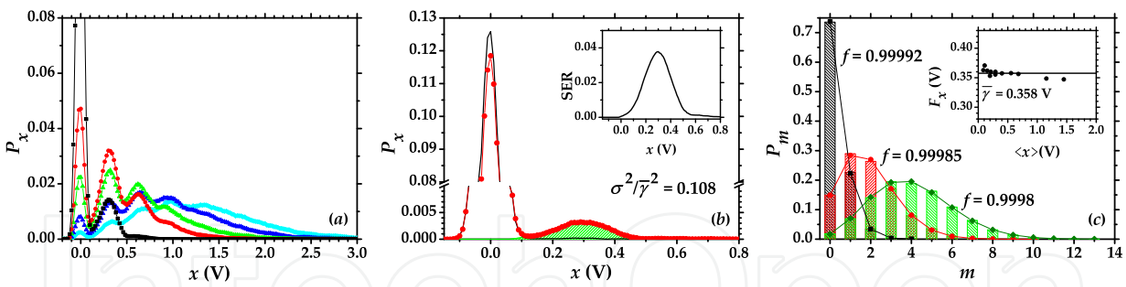

Fig. 2. (*a*) Typical pulse-height spectra measured with the $\mathrm{PMT}_{\mathrm{Burle}}$ at different light intensities. (*b*) Estimation of the single-electron response (SER) of the detector by subtraction of the response to the dark from the response to a very weak light. Note the interruption in the vertical axis. Inset: normalized SER. (*c*) Inset: Plot of the Fano factor, F_x, for the output voltages as a function of the mean voltage $\langle x \rangle$ for coherent states having different intensities (dots) and linear fit (line). Main panel: Reconstructed distribution, $P_{m,\mathrm{exp}}$, for coherent light reconstructed from some of the data sets used to obtain the calibration in the Inset (bars). Line+symbols: theoretical curves, P_m, from Equation (11).

To evaluate the applicability of the theory described above to the detector, we introduce a simple analysis of its response to obtain an estimation of the SER. We consider the normalized pulse-height spectrum P_x produced by very low illumination, virtually in the so-called "single-photon regime" (red line+dots in Fig. 2(*b*)) and subtract from it a fraction of the normalized pulse-height spectrum obtained in the dark (black line). We interpret the resulting curve obtained by varying the fraction until we get a single peak (green area) as p_γ, *i.e.* the SER of the system. The inset shows the normalized SER together with the evaluation of $\sigma^2/\overline{\gamma}^2 \sim 0.108$, a value that suggests the applicability of our analysis method.
In Fig. 2(*c*) we show the application of the analysis technique to the recorded data. In the inset of the figure we plot the Fano factor of the outputs (dots) along with the linear fit, that gives $\overline{\gamma} = (0.358 \pm 0.002)$ V, while in the main panel we show the experimental distributions $P_{m,\mathrm{exp}}$ (bars) reconstructed by using $\overline{\gamma}$ along with the theoretical curves P_m evaluated at the measured mean values. The values of the fidelity reported in the figure indicate the good quality of the reconstructions.

3.2 Hybrid photodetector

The second detector we tested is the H8236-40 hybrid photodetector (HPD, Hamamatsu, Japan). The light-sensitive element of the detector is a GaAsP(Cs) photocathode (maximum $QE = 0.40$ at $\sim$550 nm). Instead of a series of dynodes, the detector incorporates a semiconductor element into an evacuated electron tube. The photoelectrons emitted by the photocathode are accelerated and strike the semiconductor undergoing multiplication. Since the fluctuation in the multiplication process is very low, the HPD displays high electron resolution and excellent stability. The HPD has negligible dark-count rate and after-pulse probability. In Fig. 3(*a*) some typical pulse-height spectra taken at different light intensities are shown. We note that the HPD has a partial peak resolution, but again the peak structure disappears as soon as the field intensity becomes mesoscopic, even if the detector remains linear in the mean values over a wide range of intensities. The estimation of the SER of the HPD (see Fig. 3(*b*)) gives a value of $\sigma^2/\overline{\gamma}^2 \sim 0.126$, that is still small enough to apply the theory. The results for the reconstructed distributions are shown in Fig. 3(*c*): in the inset we

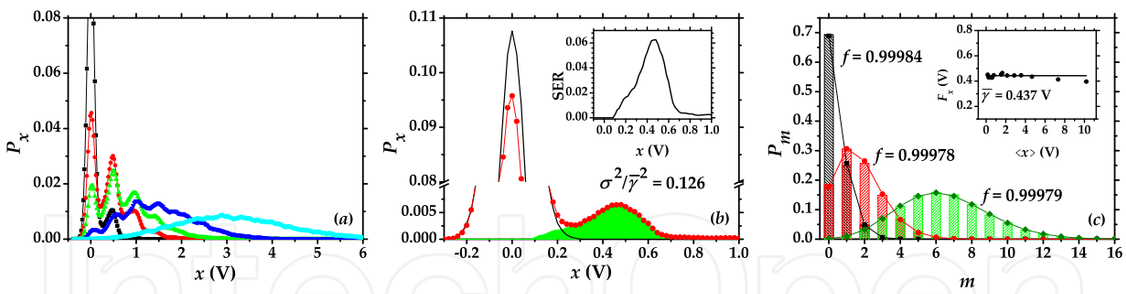

Fig. 3. Same as in Fig. 2 for HPD.

show the experimental results for the Fano factor of the output F_x (dots) and the linear fit that gives $\overline{\gamma} = (0.437 \pm 0.005)$ V, while in the main panel we show the reconstructed distributions and the theoretical curves. The fidelity is very high.

3.3 Single-photon-counting photomultiplier

We now check the theoretical description with a H5773P photomultiplier ($\text{PMT}_{\text{single}}$, Hamamatsu, Japan) that has no photon-number resolving power but that can be used for single-photon counting in that its output for zero detected photons can be discriminated from SER. According to the specifications, for light pulses of duration well below its time response (typical rise time: 0.78 ns) delivered at kHz repetition rate as in our experiments, the $\text{PMT}_{\text{single}}$ should saturate for m-values of few units. The $\text{PMT}_{\text{single}}$ current output was processed by an amplifier (ZFL 1000NL, Mini-Circuits) and integrated by a charge digitizer (V792, CAEN) with a 12-bit resolution over a temporal gate (40 ns) synchronized by means of the Q-switching signal of the laser amplifier. The final x outputs obtained for each ensemble of 30000 light pulses were then recorded by a computer.

The pulse height spectra in Fig. 4(a) at increasing light intensity show that the PMT has no photon-number resolving power, being just able to distinguish between $m = 0$ and $m > 0$. From the estimation of the SER in Fig. 4(b), we see that the response of the $\text{PMT}_{\text{single}}$ has

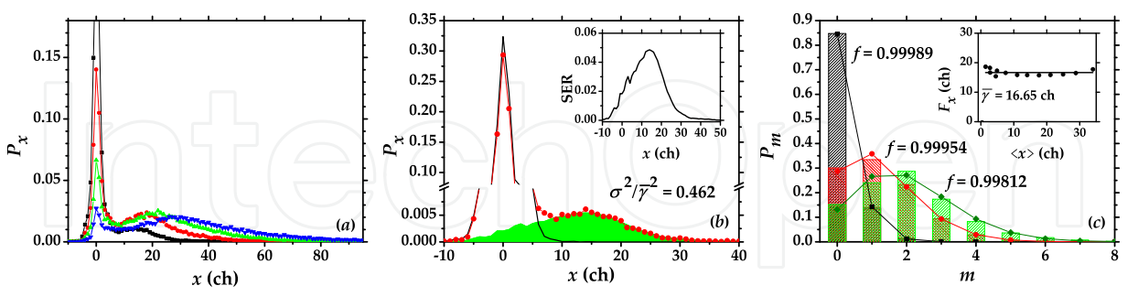

Fig. 4. Same as in Fig. 2 for $\text{PMT}_{\text{single}}$ detector.

$\sigma^2/\overline{\gamma}^2 \sim 0.462$, a value that could still be low enough to apply the theory.

In the inset of Fig. 4(c), we report the value of the Fano factor of the output $\overline{\gamma} = (16.7 \pm 0.3)$ ch. According to the main panel of Fig. 4(c), we are able to reconstruct detected photon distributions P_m with high fidelity for mean values slightly above $\langle m \rangle = 2$, that is when the probability of detecting photons, in the case of Poissonian statistics, remains non-negligible up

to $m = 7$. We remark that this result is achieved by using a PMT that can hardly distinguish between $m = 0$ and $m = 1$.

3.4 Proportional photomultiplier

Finally, we want to demonstrate that the condition $\sigma^2/\overline{\gamma}^2 \ll 1$ is actually necessary for a detector to be used to reconstruct the photon-number statistics by measuring shot-by-shot photon numbers. To this aim we used a 931B photomultiplier (PMT, Hamamatsu, Japan) that is endowed with a very poor photon-number resolution (see Fig. 5(*a*)). Although the detector

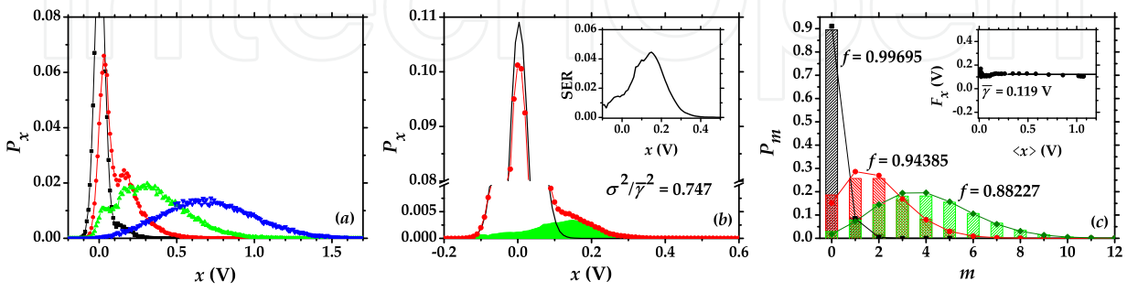

Fig. 5. Same as in Fig. 2 for $\mathrm{PMT}_{\mathrm{prop}}$ detector.

does not resolve even the first terms in Equation (2) as separate peaks, we try to recover its SER (see Fig. 5(*b*)). The obtained value of $\sigma^2/\overline{\gamma}^2 \sim 0.747$ confirms the expected non-applicability of the analysis method.

If we apply our procedure to the measurements performed on coherent light, we obtain the results displayed in Fig. 5(*c*): the value of γ obtained from the fit of the Fano factor (see inset) produces reconstructed statistical distributions having a limited fidelity with the expected theoretical distributions evaluated at the experimental mean values (see main panel).

4. Applications

We exploited the capability of the HPD described above, assisted by the analysis technique, for some different applications. First of all we retrieved the P_m distributions for light states having different photon-number statistics. Secondly, we used the measured statistics to reconstruct the Wigner function of some classical optical states. Third, we demonstrated that we can measure shot-by-shot photon-number correlations between bipartite states and finally we used correlations to produce conditional non-Gaussian states.

4.1 Statistics

We produced a number of "artificial" field states by mixing, at a beam splitter, different fields generated by a pulsed laser source (Bondani et al., 2009c). Here we show the results obtained for two of such states, the displaced thermal state and the phase-averaged coherent state, which are relevant for the applications described in Section 4.2. As displayed in Fig. 6(*a*), both these states were obtained by mixing two fields at a beam splitter (BS). To obtain the displaced thermal state, we produced a single-mode thermal state containing n_{th} mean photons by inserting a rotating ground glass plate (D) and selecting a single speckle by a pin-hole (PH). Then we mixed the single-mode thermal field with a coherent field containing $|\alpha|^2$ mean photons at the BS, thus implementing the displacement operation. The resulting state is

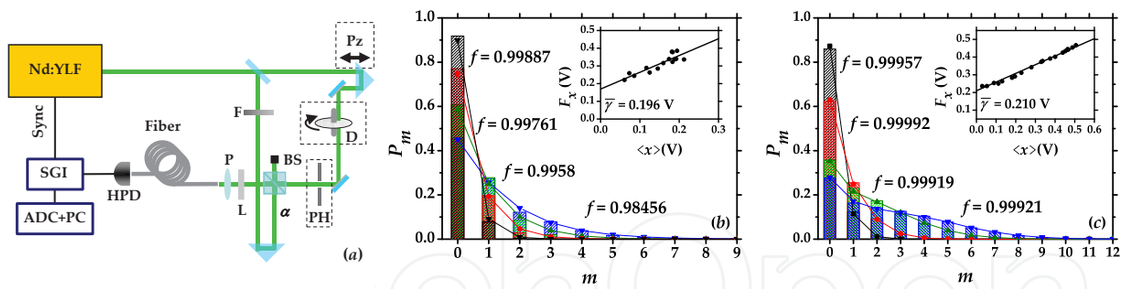

Fig. 6. (*a*) Experimental setup for the generation and measurement of either a displaced single-mode thermal state or a phase-averaged coherent state. Dashed boxes: elements inserted to obtain the different states. (*b*) Displaced single-mode thermal state. Inset: Fano factor, F_x, as a function of $\langle x \rangle$. Main panel: reconstructed detected-photon distributions for some of the data sets used to calculate the Fano factor (bars) and theoretical curves (lines+symbols). (*c*) Same as (*b*) for phase-averaged coherent state.

described by the following photon-number distribution

$$P_n = \frac{n_{\rm th}^n}{(n_{\rm th}+1)^{n+1}} \exp\left(-\frac{|\alpha|^2}{n_{\rm th}+1}\right) L_n\left(-\frac{|\alpha|^2}{n_{\rm th}(n_{\rm th}+1)}\right), \tag{14}$$

in which L_n is the Laguerre polynomial L_n^γ for $\gamma = 0$. We have $\langle n \rangle = n_{\rm th} + |\alpha|^2$, $\mu_2(n) = n_{\rm th} + |\alpha|^2 + n_{\rm th}\left(n_{\rm th} + 2|\alpha|^2\right)$ and hence, according to Equation 10, we get $F_x = K\langle x \rangle + \overline{\gamma}$, with $K = n_{\rm th}\left(n_{\rm th} + 2|\alpha|^2\right) / \left(n_{\rm th} + |\alpha|^2\right)^2$.
In Fig. 6(*b*) we plot the experimental results for a number of reconstructed distributions (bars) along with the theoretical distributions calculated from Equation 14. In the inset, we show the values of F_x as a function of $\langle x \rangle$.
The phase-averaged coherent state was obtained by superimposing two coherent fields whose relative phase was randomized from shot to shot. We obtained phase randomization by changing the path of one of the two fields at a frequency of ∼100 Hz with a piezoelectric device, Pz, covering a travel length of 1.28 μm (see Fig. 6(*a*)). If the two coherent states contain $|\alpha|^2$ and $|\alpha_0|^2$ mean photons, the photon-number distribution is (Zambra et al., 2007)

$$P_n = \frac{A^n e^{-A}}{2\pi n!} \sum_{k=0}^{n} \binom{n}{k} \left(-\frac{B}{A}\right)^k \frac{\Gamma(1/2+k/2)\,\Gamma(1/2)}{\Gamma(1+k/2)} {}_1F_2\left[\left\{\frac{1}{2}+\frac{k}{2}\right\}, \left\{\frac{1}{2}, 1+\frac{k}{2}\right\}, \frac{B^2}{4}\right] \tag{15}$$

where $A = |\alpha|^2 + |\alpha_0|^2$, $B = 2|\alpha||\alpha_0|$ and ${}_1F_2(a,b,z)$ is the generalized hypergeometric function. We get $\langle n \rangle = |\alpha|^2 + |\alpha_0|^2$, $\mu_2(n) = \langle n \rangle \left(K'\langle n \rangle + 1\right)$, with $K' \equiv 2|\alpha|^2|\alpha_0|^2/(|\alpha|^2 + |\alpha_0|^2)^2$ and $F_x = K'\langle x \rangle + \overline{\gamma}$.
In Fig. 6(*c*) we plot the experimental results for a number of reconstructed distributions (bars) along with the theoretical distributions calculated from Equation 15 and the values of the Fano factor for outputs (inset).

4.2 Wigner function

The capability of reliably reconstructing generic light states can be exploited to directly reconstruct the Wigner function of a state (Banaszek & Wodkiewicz, 1996; Banaszek et al., 1999; Cahill & Glauber, 1969; Wallentowitz & Vogel, 1996), with a technique alternative to OHT. The method consists in detecting the light exiting a beam-splitter that mixes the signal

with a variable coherent probe field (see Fig. 6(*a*)). The Wigner function of the state can be written as

$$W(\alpha) = \frac{2}{\pi} \sum_{n=0}^{\infty} (-1)^n P_{n,\alpha} \ , \tag{16}$$

where $P_{n,\alpha}$ is the photon-number distribution of the field displaced by α. To obtain the photon-number distribution, reconstruction/inversion methods must be implemented (Allevi et al., 2009a) that require a known and sufficiently high photon-detection efficiency (Kiss et al., 1995). If, instead of $P_{n,\alpha}$, we consider $P_{m,\beta}$, the distribution of detected photons, where $\beta = \sqrt{\eta}\alpha$ is the detected amplitude of the displacement field, we obtain the Wigner function in the presence of losses (Banaszek & Wodkiewicz, 1996)

$$\overline{W}(\beta) = \frac{2}{\pi(1-\eta)} \int d^2\beta' e^{-\frac{2}{1-\eta}|\beta-\beta'|^2} W(\beta'/\sqrt{\eta}) = \sqrt{2}\pi \sum_{m=0}^{\infty} (-1)^m P_{m,\beta} \tag{17}$$

where $W(\beta/\sqrt{\eta}) = W(\alpha)$ is the Wigner function for photons. It can be demonstrated that,

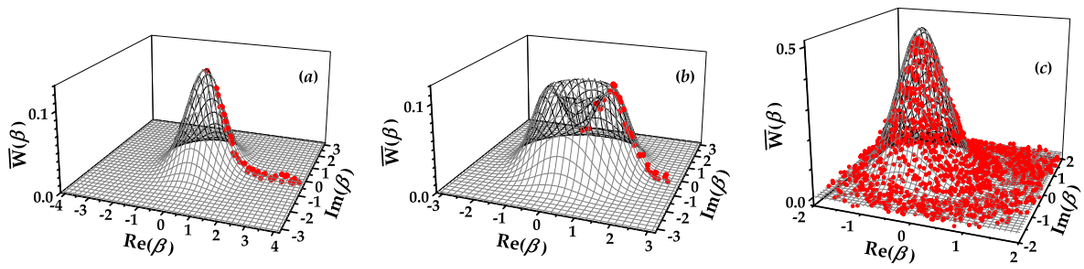

Fig. 7. Reconstructed Wigner functions (dots) superimposed to their theoretical surfaces for (*a*): single-mode thermal state, (*b*): phase-averaged coherent state and (*b*) coherent state.

for classical states such as non-squeezed Gaussian states and their linear superpositions, the integral in Equation (17) preserves the functional form of the Wigner distribution, so that the information directly extracted from detected photons is enough to characterize the state.

We used the experimental setups in Fig. 6(*a*) but with a frequency-doubled Q-switched Nd:YAG laser at 15 kHz repetition rate (Quanta System) delivering pulses at 532 nm of $\sim$ 200 ns duration as the laser source. The beam was spatially filtered and split into two parts serving as signal and probe fields. The probe was left Poissonian while that of the signal was modified in order to get the different states to be measured. The probe, whose intensity was modified by a variable neutral density filter, was then mixed with the signal at the PBS.

We begin by considering the reconstruction of the Wigner function of the two states considered in Section 4.1, the single-mode thermal state and the phase-averaged coherent state. Since both these states are phase-insensitive, their Wigner function is symmetric with respect to the origin and thus it is not necessary to control the phase of the probe field. In Fig. 7 we plot the reconstructed Wigner function for a single-mode thermal field (*a*) and for the phase-averaged coherent field (*b*). The dots in the figure are the experimental data and the surface is the theoretical Wigner function evaluated at the experimental parameters including some corrections that account for the mode-mismatching between probe and signal (Bondani et al., 2009b).

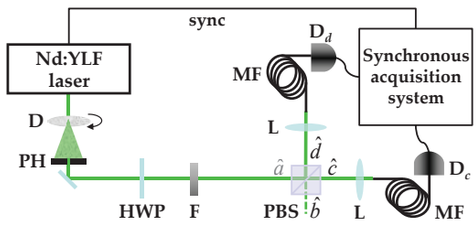

Fig. 8. Scheme of the experimental setup for the measurement of shot-by-shot correlations in single-mode thermal fields.

As an example of reconstruction of the Wigner function of a phase-sensitive state, we consider a coherent state. To perform the measurements we varied the phase of the probe field by means of a piezoelectric movement and evaluated the actual values of the phase by exploiting the linearity properties of the HPD (Bondani et al., 2010). In Figure 7(*c*) we plot the resulting Wigner function.

4.3 Correlations

Till now, we have demonstrated that HPDs are endowed with the capability of reconstructing the correct statistics of detected photons provided their outputs are analyzed in the proper way (Bondani et al., 2009a;b;c). Now we exploit the fact that, in principle, our analysis allows us to determine the number of photons detected at each laser shot correctly enough to reveal shot-by-shot photon-number correlations between the components of a bipartite state. We tested measurement apparatus and procedure by measuring the correlations in a classically-correlated bipartite state, namely a single-mode thermal field divided by a beam-splitter. The two HPDs used in these measurements were model R10467U-40 (Hamamatsu, Japan). According to the experimental setup sketched in Fig. 8, we produced a single-mode thermal field as described in Section 4.1. The selected mode was then sent to a polarizing beam-splitter (PBS) whose outputs were collected by two multimode fibers and delivered to the detectors. To obtain a fine tuning of the beam-splitter transmittance we inserted a half-wave plate (HWP) between the PH and the PBS. The light pulses were then delivered to the detectors ($D_{c,d}$) through two multimode fibers (MF). Single-shot detector outputs were then amplified, integrated, digitized and recorded. We measured 30000 subsequent shots at a number of different intensity values set by a variable neutral density filter (F). In Fig. 9(*a*) we plot the joint probability distributions obtained by re-scaling the outputs of the detectors by the proper value of $\overline{\gamma}$ without rebinning the data.

Referring to Fig. 8, the field operators at the outputs of the beam splitter ($\hat{c}$ and $\hat{d}$) are linked to the input ones ($\hat{a}$ and $\hat{b}$) by $\hat{c} = \sqrt{\tau}\hat{a} - \sqrt{1-\tau}\hat{b}$ and $\hat{d} = \sqrt{1-\tau}\hat{a} + \sqrt{\tau}\hat{b}$, τ being the beam splitter transmittance. If $\hat{b}$ is in the vacuum, the moments of the bipartite state at the output are given by $\langle \hat{n}_c \rangle = \tau \langle \hat{n}_a \rangle$, $\sigma^2_{n_c} = \tau \left[\tau \sigma^2_{n_a} + (1-\tau)\langle \hat{n}_a \rangle \right]$, $\langle \hat{n}_d \rangle = (1-\tau)\langle \hat{n}_a \rangle$, $\sigma^2_{n_d} = (1-\tau)\left[(1-\tau)\sigma^2_{n_a} + \tau \langle \hat{n}_a \rangle \right]$ and $\langle \hat{n}_c\, \hat{n}_d \rangle = \tau(1-\tau)\left(\langle \hat{n}^2_a \rangle - \langle \hat{n}_a \rangle \right)$, from which we obtain the expression for the normalized correlation coefficient:

$$\Gamma \equiv \frac{\langle (n_c - \langle \hat{n}_c \rangle)\,(n_d - \langle \hat{n}_d \rangle) \rangle}{\sigma^2_{n_c} \sigma^2_{n_d}} = \frac{\sqrt{\tau(1-\tau)}\left[\sigma^2_{n_a} - \langle \hat{n}_a \rangle \right]}{\sqrt{\left[\tau \sigma^2_{n_a} + (1-\tau)\langle \hat{n}_a \rangle \right]\left[(1-\tau)\,\sigma^2_{n_a} + \tau \langle \hat{n}_a \rangle \right]}} \,. \tag{18}$$

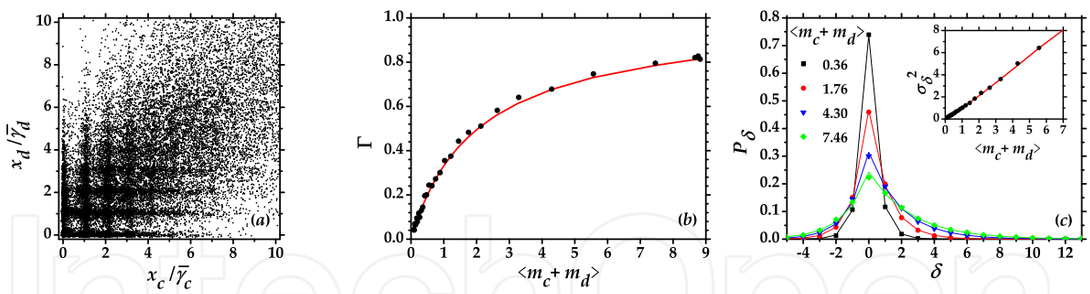

Fig. 9. (*a*) Experimental joint probability distribution. (*b*) Shot-by-shot correlation, Γ, as a function of the total mean value. (*c*) Experimental results for P_δ (symbols) and theoretical predictions (full lines). Inset: measured variance σ_δ^2 of P_δ as a function of the total number of detected photons (dots) and theoretical prediction (full line).

The single-mode thermal state at the input port *a* of the PBS can be written as

$$\nu_{n_{\rm th}} = \sum \frac{n_{\rm th}^n}{(1+n_{\rm th})^{n+1}} |n\rangle\langle n| = \sum_n P_n |n\rangle\langle n| \tag{19}$$

and obviously $\langle \hat{n}_a \rangle = n_{\rm th}$. Equation 18 becomes

$$\Gamma = \frac{\sqrt{\tau(1-\tau)n_{\rm th}^2}}{\sqrt{(\tau n_{\rm th}+1)[(1-\tau)n_{\rm th}+1]}} = \frac{\sqrt{\langle n_c\rangle\langle n_d\rangle}}{\sqrt{(\langle n_c\rangle+1)(\langle n_d\rangle+1)}}, \tag{20}$$

where $\langle n_c \rangle = \langle \hat{n}_c \rangle$ and $\langle n_d \rangle = \langle \hat{n}_d \rangle$. If the overall detection efficiencies are $\eta_{c,d}$, the expression in Equation (20) remains the same upon substituting the mean number of photons $\langle n_{c,d} \rangle$ with that of detected photons $\langle m_{c,d} \rangle = \eta_{c,d} \langle n_{c,d} \rangle$ (Agliati et al., 2005). Figure 9(*b*) shows the results for shot-by-shot correlation measured as a function of the total mean value of the output detected light $\langle m_c + m_d \rangle$. Full line represent the theoretical curve evaluated according to Equation (20) by inserting the experimental mean values. The results obtained with HPDs perfectly superimpose to the theory.

Relevant applications of correlated bipartite states require the determination of the nature of the correlations. A quite standard way to discriminate between classical and nonclassical states (Agliati et al., 2005) is to study the statistics of the difference, P_δ, in the number of photons detected shot-by-shot at the outputs of the beam splitter. Figure 9(*c*) displays the experimental results for P_δ evaluated by subtracting the number of detected photons measured shot-by-shot together with the theoretical values evaluated according to Ref. (Agliati et al., 2005). The inset of the figure displays the measured variance σ_δ^2 as a function of the total number of detected photons, as compared to the theoretical predictions $\sigma_\delta^2 = (\langle m_c \rangle - \langle m_d \rangle)^2 + \langle m_c \rangle + \langle m_d \rangle$ (Agliati et al., 2005). The correct evaluation of σ_δ^2 is crucial for the estimation of the noise reduction in a bipartite state $R = \sigma_\delta^2 / (\langle m_c \rangle + \langle m_d \rangle)$, which is a means to discriminate classical from nonclassical states. The results superimpose to the theory.

4.4 Conditional states

Nonclassical optical states are a crucial ingredient for fundamental tests of quantum mechanics and represent a resource for quantum communication and high-precision measurements. Besides squeezing, nonclassical effects are generally observed in connection

with non-Gaussian states of light. It has been demonstrated that non-Gaussian states and operations represent a valuable resource for Quantum Information (Genoni et al., 2010): in fact, they have been studied in connection with entanglement distillation (Aoki et al., 2009; Dong et al., 2008; Eisert et al., 2002; Fiurasfiek, 2002), teleportation (Cochrane et al., 2002; Olivares et al., 2003; Opatrny et al., 2000), cloning (Cerf et al., 2005) and quantum storage (Casagrande et al., 2007). The simplest way to generate a non-Gaussian optical state starting from a Gaussian one consists in subtracting photons from it (Ourjoumtsev et al., 2007; Parigi et al., 2009), an operation that can be implemented by inserting a beam splitter in the optical path of the original state, detecting the number of photons at one output port and selecting the output of the other port only if a certain condition on the number of detected photons is satisfied. When short-pulsed fields are used, the challenging part of this scheme is the shot-by-shot measurement of sizeable numbers of photons.

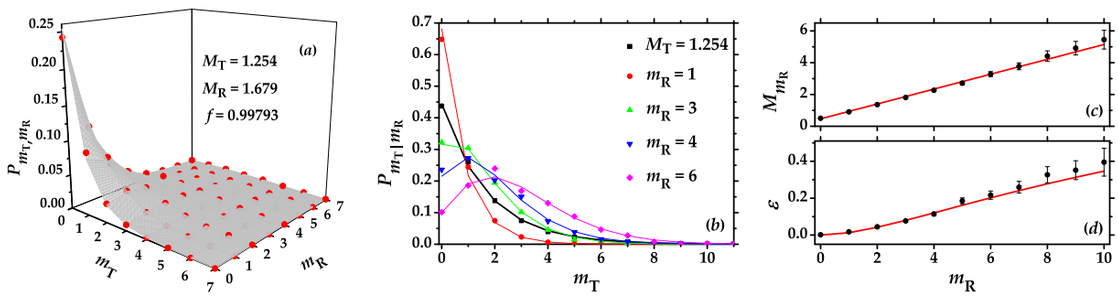

Fig. 10. (*a*) Joint detected-photon distribution: the experimental data are plotted as dots and the theoretical surface as grey mesh. (*b*) Reconstructed distributions of different conditional states (colored symbols) obtained starting from the same unconditioned one (black squares). The theoretical curves are plotted as lines according to the same choice of colors. (*c*) Mean number of detected photons of the conditional states and (*d*) Lower bound of non-Gaussianity measure, plotted as functions of the conditioning value (experimental data (dots) and theoretical curve (solid line)).

Here we present the production and characterization of non-Gaussian states of light starting from both classically and quantum correlated optical fields and exploiting the characteristics of the HPDs. First of all, we report the results obtained by using single-mode thermal fields as input states (Allevi et al., 2010b). Though photon-subtracted thermal states are not directly involved in any quantum information protocol, they are suitable probes to investigate the performances of our particular scheme. In fact, thermal states are Gaussian states diagonal in the photon-number basis, thus, the knowledge of their photon statistics fully characterizes them and their conditional non-Gaussian counterparts, which are still diagonal. Thanks to this property, we can give a complete analytical description of the behavior of the setup, including the actual expressions of the conditional states, and we can verify, with very high accuracy and control, the agreement of the theoretical expectations with the experimental results. We refer to the experimental setup sketched in Fig. 8, in which the input state at the PBS is the single-mode thermal state $\nu_{n_{\rm th}}$ and the transmitted and reflected fields are described by the operators $\hat{c}$ and $\hat{d}$, respectively. The measurements performed in the reflected beam irreversibly modify the states measured in the transmitted arm and, in particular, make them non-Gaussian. As an example, here we show the results obtained by choosing a set of measurements with $\langle m_c \rangle = \mathrm{M_T} \sim 1.254$. The joint probability $P_{m_{\rm T},m_{\rm R}}$ of measuring $m_{\rm R}$ photons in the reflected arm and $m_{\rm T}$ photons in the transmitted one is plotted in Fig. 10(*a*) as

dots together with the theoretical surface to which it perfectly superimposes. Starting from the theoretical joint probability, we can calculate the expected photon-number distribution of the states obtained by performing different conditional measurements in the reflected arm. As it is shown in panel (*b*) of Fig. 10, the larger the conditioning value, the more different the statistics of the conditional state (lines + symbols) is from that of the incoming one (black squares + line). The accordance with the theoretical expectation, which can be quantified by calculating the fidelity (see f values in the figure), is rather satisfactory. In Fig. 10(*c*), we also plot the behavior of the mean number of photons of the conditional states as a function of the different conditioning values m_{R}. Finally, to deeply characterize the output conditional states we define the non-Gaussianity measure as

$$\delta = S[\nu_{N_{n_{\mathrm{R}}}}] + \sum_n P_n \log P_n \tag{21}$$

where $N_{n_{\mathrm{R}}}$ is the mean photon number of the conditional states, and $S[\nu_{n_{\mathrm{th}}}] = n_{\mathrm{th}} \log(1 + 1/n_{\mathrm{th}}) + \log(1 + n_{\mathrm{th}})$ is the entropy of the single-mode thermal state $\nu_{n_{\mathrm{th}}}$ (see Equation 19). However, due to the inefficient detection, we cannot reconstruct the actual photon-number distribution P_n, but only the detected-photon-number distribution $P_{m_{\mathrm{T}},m_{\mathrm{R}}}$. Remembering that for thermal states the statistics of detected photons is still thermal, we evaluate the quantity

$$\varepsilon = S[\nu_{M_{m_{\mathrm{R}}}}] + \sum_{m_{\mathrm{T}}} P_{m_{\mathrm{T}},m_{\mathrm{R}}} \log P_{m_{\mathrm{T}},m_{\mathrm{R}}} \leq \delta. \tag{22}$$

The last inequality follows from the fact that the inefficient detection may be described by a Gaussian lossy channel that does not increase the non-Gaussianity, followed by an ideal (*i.e.* unit quantum efficiency) detection. The quantity ε turns out to be a lower bound for the actual non-Gaussianity, that is, significant values of ε correspond to more markedly non-Gaussian states. The behavior of ε as a function of the conditioning value m_{R} predicted by the theory (line) is well reproduced by the experimental data (dots) shown in Fig. 10(*d*).

As a second application, we address multimode conditional measurements on the quantum correlated optical states produced by a pulsed multimode spontaneous parametric down-conversion (Allevi et al., 2010c).

The experimental setup is sketched in Fig. 11(*a*). The pump light source was the fourth harmonics of a Nd:YLF ps-pulsed laser (High-Q Laser Production, Austria) produced by a non-collinear sum-frequency generation. The pump was then sent into a β-BaB_2O_4 (BBO) crystal (Kaston, China, cut angle 48.84 deg, 4 mm length) to produce pairwise entanglement at 523.5 nm, in order to match the maximum quantum efficiency ($QE = 0.5$) of the HPDs. The UV stray light was cut-off by a filter and by two harmonic separators. Signal and idler were selected by two pin-holes (300 μm diameter, located at 1 m from BBO2). Notice that the number of temporal modes, which is evaluated from the marginal detected-photon number distribution, cannot be reduced at will. The only way to reduce the number of modes is to select a single spatial mode, which involves the challenging matching of the collection areas in signal and idler. The possible mismatch between the collection areas results in an effective detection efficiency, reduced in comparison to the nominal efficiency of the detectors, which can be estimated through the level of noise reduction $R = 1 - \eta$ (see Fig. 11(*c*)) exhibited by the two beams (Bondani et al., 2007). For our beams we obtained, without noise subtraction, $\eta \sim 0.06$. The light passing the pin-holes was coupled to two multimode optical fibers and delivered to the detectors. Each experimental run was performed on 50000 subsequent laser

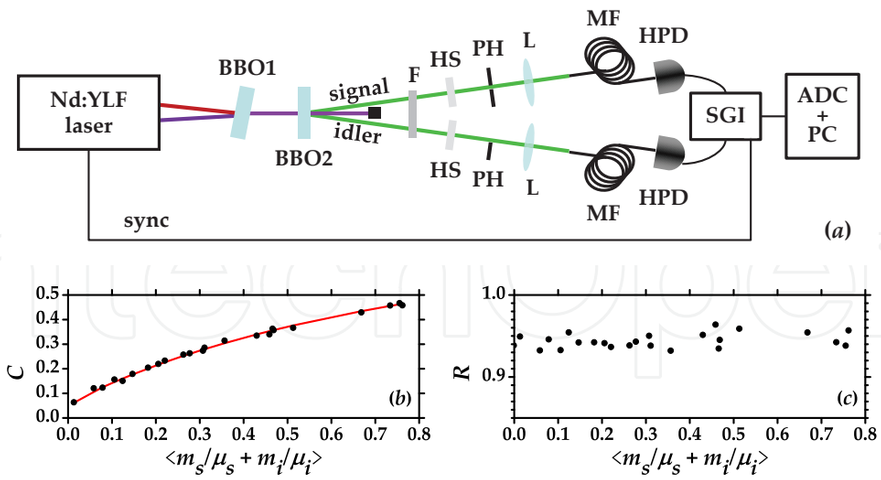

Fig. 11. (*a*) Schematic diagram of the experimental setup. BBO1 and BBO2: nonlinear crystals; F: cut-off filter; HS: harmonic separators; PH: pin-hole apertures; L: lenses; MF: multimode optical fibers; HPDs: amplified hybrid photodetectors; SGI: synchronous gated integrator; ADC+PC: digitizing PC board. (*b*) Detected-photon correlation coefficient and (*c*): shot-noise reduction, plotted as functions of the mean number of detected photons per mode (experimental data (dots) and theoretical curve (solid line)).

shots at fixed values of the pump intensity. First of all, we characterized the entangled states by measuring the correlation coefficient

$$C = \frac{\sqrt{(M_s/\mu_s)(M_i/\mu_i)} + \eta}{(M_s/\mu_s + 1)(M_i/\mu_i + 1)}, \tag{23}$$

where $M_{s,i}$ is the mean number of detected photons and $\mu_{s,i}$ is the number of modes in signal and idler. In Fig. 11(*b*) we plot C as a function of the total mean number of detected photons per mode: the experimental results are in perfect accordance with theory.
For what concerns the generation of non-Gaussian states, we notice that the intrinsic multimode nature of our entangled states makes the theoretical description of the photon-subtracted states non trivial. Moreover, a quantification of the amount of non-Gaussianity is not possible, as all the existing descriptions refer to single-mode states (Genoni & Paris, 2010). The experimental joint detected-photon distribution P_{m_s,m_i}, plotted in Fig. 12(*a*), is well superimposed to the theoretical curve derived from the multimode description of the process. Starting from its expression we calculated the photon distribution of the conditional states obtained by choosing the values of the measured photons on the idler beam, m_i. Panel (*b*) of Fig. 12 displays the detected-photons distributions of the conditional states obtained by choosing a definite number of detected photons on the idler ($m_i = 10$ and $m_i = 15$). We notice that the results are in excellent agreement with the theory and, despite the small value of effective quantum efficiency, the conditioning power of the measurement is appreciable. This is clearly illustrated by the behavior of the mean values of the distributions, which is reported in panel (*c*) of Fig. 12 as a function of the conditioning value: the experimental data are again in agreement with the theoretical prediction.
The conditioning protocol is thus effective even though the results are somehow limited by the specific characteristics of the original twin-beam state and in particular by its multimode

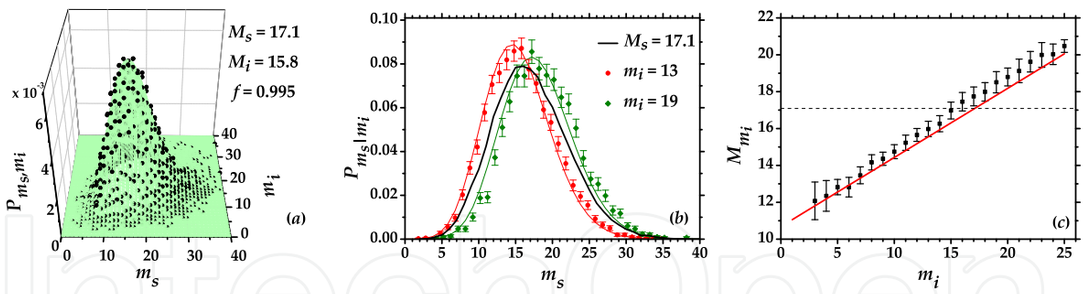

Fig. 12. (*a*) Joint detected-photon distribution: the experimental data are plotted as dots and the theoretical surface as grey mesh. (*b*) Reconstructed distributions of two different conditional states (symbols) obtained starting from the same unconditioned one (black line). The theoretical curves are plotted as lines according to the same choice of colors. (*c*) Mean number of detected photons of the conditional states as a function of the conditioning value: experimental data (dots) and theoretical curve (solid line). The dashed line corresponds to the mean value of the unconditioned state.

nature. The results could be improved by decreasing the number of temporal modes, either by reducing the pump duration or by changing the nonlinear crystal: work is in progress to follow both these lines.

5. Conclusions

We have presented the generation and characterization of pulsed optical states in the mesoscopic photon-number regime. In particular, the good results obtained for the reconstruction of detected-photon distributions and Wigner functions, for the measurement of shot-by-shot photon-number correlations and for the implementation of multiple photon-subtraction by means of HPDs open the way to the exploitation of these detectors for several applications in the fields of Quantum Optics and Quantum Information. Their main power is represented by the possibility to provide all the information contained in each laser shot, which is a required feature for the implementation of quantum communication protocols. The satisfactory experimental results obtained till now with classical states encourage us to explore more exotic classical states, such as the non-Gaussian ones, that could be useful as probe fields in many application schemes.
Nevertheless, beside the many advantages, we are conscious that the HPDs present an intrinsic deviation from ideality in the single-electron response. This limitation seems to be irrelevant for classical states, but becomes critical in case of detection of nonclassical states, as the uncertainty in the determination of the photon peaks corresponds to a reduction of the overall quantum efficiency. In order to minimize this problem, we could try to increase the gain of the detection chain by operating the HPDs at the maximum voltage below the breakdown threshold and at the minimum temperature allowed, and to refine the analysis of the detector outputs to include this effect in the description of its response.

6. References

Afek, I.; Natan, A.; Ambar, O., & Silberberg, Y. (2009). Quantum state measurements using multipixel photon detectors. *Phys. Rev. A.*, Vol. 79, No. 4, April 2009, 043830, ISSN 1050-2947.

Agliati, A.; Bondani, M.; Andreoni, A.; De Cillis, G., & Paris, M. G. A. (2005). Quantum and classical correlations of intense beams of light investigated via joint photodetection. *J. Opt. B Quantum Semiclass. Opt.*, Vol. 7, No. 12, November 2005, S652–S663, ISSN 1464-4266.

Akindinov, A. V.; Martemianov, A. N.; Polozov, P. A.; Golovin, V. M., & Grigoriev, E. A. (1997). New results on MRS APDs. *Nucl. Instr. and Meth. in Phys. Res. A*, Vol. 387, No. 1-2, March 1997, 231–234, ISSN 0168-9002.

Allevi, A.; Andreoni; Bondani, M.; Brida, G.; Genovese, M; Gramegna, M.; Olivares, S.; Paris, M. G. A.; Traina, P., & Zambra, G. (2009). State reconstruction by on/off measurement. *Phys. Rev. A*, Vol. 80, No. 2, August 2009, 022114, ISSN 1050-2947.

Allevi, A.; Bondani, M., & Andreoni, A. (2010). Photon-number correlations by photon-number resolving detectors. *Opt. Lett.*, Vol. 35, No. 10, May 2010, 1707–1709, ISSN 0146-9592.

Allevi, A.; Bondani, M.; Andreoni, A.; Genoni, M. G., & Olivares, S. (2010). Reliable source of conditional states from single-mode pulsed thermal fields by multiple-photon subtraction. *Phys. Rev. A*, Vol. 82, No. 1, July 2010, 013816, ISSN 1050-2947.

Allevi, A.; Andreoni, A.; Bondani, M.; Beduini, F. A.; Genoni, M. G.; Olivares, S., & Paris, M. G. A. (2010). Conditional measurements on multimode pairwise entangled states from spontaneous parametric downconversion. *Europhys. Lett.*, Vol. 92, No. 2, October 2010, 20007, ISSN 0295-5075.

Andreoni, A. & Bondani, M. (2009). Photon statistics in the macroscopic realm measured without photon counters. *Phys. Rev. A*, Vol. 80, No. 1, July 2009, 013819, ISSN 1050-2947.

Andreoni, A.; Allevi, A., & Bondani, M. (2009). Mesoscopic photon-number statistics measured with a non-counting PMT. *J. Russ. Laser Res.*, Vol. 30, No. 5, September 2009, 418–426, ISSN 1071-2836.

Aoki, T.; Takahashi, G.; Kajiya, T.; Yoshikawa, J.; Braunstein, S. L.; van Loock, P., & Furusawa, A. (2009). Quantum error correction beyond qubits. *Nat. Phys.*, Vol. 5, No. 8, August 2009, 541–546, ISSN 1745- 2473.

Arecchi, F. T. (1965). Measurement of the Statistical Distribution of Gaussian and Laser Sources. *Phys. Rev. Lett.*, Vol. 15, No. 24, December 1965, 912–916, ISSN 0031-9007.

Banaszek, K. & Wódkiewicz, K. (1996). Direct Probing of Quantum Phase Space by Photon Counting. *Phys. Rev. Lett.*, Vol. 76, No. 23, June 1996, 4344–4347, ISSN 0031-9007.

Banaszek, K.; Radzewicz, C.; Wódkiewicz, K., & Krasin'ski, J. S. (1999). Direct measurement of the Wigner function by photon counting. *Phys. Rev. A*, Vol. 60, No. 1, July 1999, 674–677, ISSN 1050-2947.

Blanchet, J.-L.; Devaux, F.; Furfaro, L., & Lantz, E. (2008). Measurement of Sub-Shot-Noise Correlations of Spatial Fluctuations in the Photon-Counting Regime. *Phys. Rev. Lett.*, Vol. 101, No. 23, December 2008, 233604, ISSN 0031-9007.

Bondani, M.; Allevi, A.; Zambra, G.; Paris, M. G. A., & Andreoni, A. (2007). Sub-shot-noise photon-number correlation in a mesoscopic twin beam of light. *Phys. Rev. A*, Vol. 76, No. 1, July 2007, 013833, ISSN 1050-2947.

Bondani, M.; Allevi, A.; Agliati, A., & Andreoni, A. (2009). Self-consistent characterization of light statistics. *J. Mod. Opt.*, Vol. 56, No. 2, January 2009, 226–231, ISSN 0950-0340 print/ISSN 1362-3044 online.

Bondani, M.; Allevi, A., & Andreoni, A. (2009). Wigner function of pulsed fields by direct detection. *Opt. Lett.*, Vol. 34, No. 9, May 2009, 1444–1446, ISSN 0146-9592.

Bondani, M.; Allevi, A., & Andreoni, A. (2009). Light Statistics by Non-Calibrated Linear Photodetectors. *Adv. Sci. Lett.*, Vol. 2, No. 4, December 2009, 463–468, ISSN 1936-6612.

Bondani, M.; Allevi, A., & Andreoni, A. (2010). Self-consistent phase determination for Wigner function reconstruction. *J. Opt. Soc. Am. B*, Vol. 27, No. 2, February 2010, 333–337, ISSN 0740-3224.

Bouwmeester, D.; Ekert, A., & Zeilinger, A. (2000). The Physics of Quantum Information, Springer-Verlag, Berlin.

Cahill, K. E. & Glauber, R. J. (1969). Density operators and quasiprobability distributions. *Phys. Rev.*, Vol. 177, No. 5, January 1969, 1882–1902.

Casagrande, F.; Lulli, A., & Paris, M. G. A. (2007). Improving the entanglement transfer from continuous-variable systems to localized qubits using non-Gaussian states. *Phys. Rev. A*, Vol. 75, No. 3, March 2007, 032336, ISSN 1050-2947.

Cerf, N. J.; Krüger, O.; Navez, P.; Werner, R. F., & Wolf, M. M. (2005). Non-Gaussian Cloning of Quantum Coherent States is Optimal. *Phys. Rev. Lett.*, Vol. 95, No. 7, August 2005, 070501, ISSN 0031-9007.

Cochrane, P. T.; Ralph, T. C., & Milburn, G. J. (2002). Teleportation improvement by conditional measurements on the two-mode squeezed vacuum. *Phys. Rev. A*, Vol. 65, No. 6, May 2002, 062306, ISSN 1050-2947.

Dong, R.; Lassen, M.; Heersink, J.; Marquardt, C.; Filip, R.; Leuchs, G., & Andersen, U. L. (2008). Experimental entanglement distillation of mesoscopic quantum states. *Nat. Phys.*, Vol. 4, No. 12, December 2008, 919–923, ISSN 1745- 2473.

Eisert, J.; Scheel, S., & Plenio, M. B. (2002). Distilling Gaussian states with Gaussian operations is impossible. *Phys. Rev. Lett.*, Vol. 89, No. 13, September 2002, 137903, ISSN 0031-9007.

Fitch, M. J.; Jacobs, B. C.; Pittman, T. B., & Franson, J. D. (2003). Photon-number resolution using time-multiplexed single-photon detectors. *Phys. Rev. A*, Vol. 68, No. 4, October 2003, 043814, ISSN 1050-2947.

Fiurášfiek, J. (2002). Gaussian transformations and distillation of entangled Gaussian states. *Phys. Rev. Lett.*, Vol. 89, No. 13, September 2002, 137904, ISSN 0031-9007.

Genoni, M. G.; Beduini, F. A.; Allevi, A.; Bondani, M.; Olivares, S., & Paris, M. G. A. (2010). Non-Gaussian states by conditional measurements. *Phys. Scr.*, Vol. 2010, No. T140, September 2010, 014007, ISSN 0031-8949.

Genoni, M. G. & Paris, M. G. A. (2010). Quantifying non-Gaussianity for quantum information. *Phys. Rev. A*, Vol. 82, No. 5, November 2010, 052341, ISSN 1050-2947.

Gol'tsman, G. N.; Okunev, O.; Chulkova, G.; Lipatov, A.; Semenov, A.; Smirnov, K.; Voronov, B.; Dzardanov, B.; Williams, C., & Sobolewski, R. (2001). Picosecond superconducting single-photon optical detector. *Appl. Phys. Lett.*, Vol. 79, No. 6, August 2001, 705–707, ISSN 0003-6951.

Gramegna, M.; Genovese, M; Brida, G.; Bondani, M.; Zambra, G.; Andreoni, A.; Rossi, A., & Paris, M. G. A. (2005). Measuring the photon distribution by ON/OFF photodectors. *Laser Physics*, Vol. 16, No. 2, February 2006, 385–392, ISSN 1054-660X.

Haderka, O.; Peřina Jr., J.; Hamar, M., & Peřina, J. (2005). Direct measurement and reconstruction of nonclassical features of twin beams generated in spontaneous parametric down-conversion. *Phys. Rev. A*, Vol. 71, No. 3, March 2005, 033815, ISSN 1050-2947.

Haderka, O.; Peřina Jr., J.; Hamar, M.; Michálek, V.; Černoch, A., & Soubusta, J. (2010). Photon-number resolving detectors. *Proceedings of SPIE 7746, 17th Slovak-Czech-Polish*

Optical Conference on Wave and Quantum Aspects of Contemporary Optics, pp. 774603, ISBN 9780819482365, Liptovsky Jan, Slovakia, September 2010, SPIE Publications.

Jozsa, R. (1994). Fidelity for Mixed Quantum States. *J. Mod. Opt.*, Vol. 41, No. 12, December 1994, 2315–2323, ISSN 0950-0340 print/ISSN 1362-3044 online.

Kim, J.; Takeuchi, S.; Yamamoto, Y., & Hogue, H. H. (1999). Multiphoton detection using visible light photon counter. *Appl. Phys. Lett.*, Vol. 74, No. 7, February 1999, 902–904, ISSN 0003-6951.

Kiss, T.; Herzog, U., & Leonhardt, U. (1995). Compensation of losses in photodetection and in quantum-state measurements. *Phys. Rev. A*, Vol. 52, No. 3, September 1995, 2433–2435, ISSN 1050-2947.

Lita, A. E.; Miller, A. J., & Nam, S. W. (2008).Counting near-infrared single-photons with 95% efficiency. *Opt. Express*, Vol. 16, No. 5, March 2008, 3032–3040, ISSN 1094-4087.

Mandel, L. & Wolf, E. (1995). *Optical Coherence and Quantum Optics*, Cambrige University Press, ISBN 0521417112, New York.

Martienssen, W & Spiller, E. (1966). Fluctuation Measurements in Mixed Light Fields. *Phys. Rev.*, Vol. 145, No. 1, May 1966, 285–287.

Olivares, S.; Paris, M. G. A., & Bonifacio, R. (2003). Teleportation improvement by inconclusive photon subtraction. *Phys. Rev. A*, Vol. 67, No. 3, March 2003, 032314, ISSN 1050-2947.

Opatrný, T.; Kurizki, G., & Welsch, D.-G. (2000). Improvement on teleportation of continuous variables by photon subtraction via conditional measurement. *Phys. Rev. A*, Vol. 61, No. 3, February 2000, 032302, ISSN 1050-2947.

Ourjoumtsev, A.; Dantan, A.; Tualle-Brouri, R., & Grangier, P. (2007). Increasing Entanglement between Gaussian States by Coherent Photon Subtraction. *Phys. Rev. Lett.*, Vol. 98, No. 3, January 2007, 030502, ISSN 0031-9007.

Parigi, V.; Zavatta, A., & Bellini, M. (2009). Implementation of single-photon creation and annihilation operators: experimental issues in their application to thermal states of light. *J. Phys. B*, Vol. 42, No. 11, June 2009, 114005, ISSN 0953-4075.

Ramilli, M.; Allevi, A.; Chmill, V.; Bondani, M.; Caccia, M., & Andreoni, A. (2010). Photon-number statistics with Silicon photomultipliers. *J. Opt. Soc. Am. B*, Vol. 27, No. 5, May 2010, 852–862, ISSN 0740-3224.

Raymer, M. G. (1997). Measuring the quantum mechanical wave function. *Contemp. Phys.*, Vol. 38, No. 5, September 1997, 343–355, ISSN 1366-5812 (electronic)/0010-7514 (paper).

Řeháček, J.; Hradil, Z.; Haderka, O., Peřina Jr., J.; & Hamar, M. (2003). Multiple-photon resolving fiber-loop detector. *Phys. Rev. A*, Vol. 67, No. 6, June 2003, 061801(R), ISSN 1050-2947.

Sansoni, L.; Sciarrino, F.; Vallone, G.; Mataloni, P.; Crespi, A.; Ramponi, R., & Osellame, R. (2010). Polarization entangled state measurement on a chip. *Phys. Rev. Lett.*, Vol. 105, No. 20, November 2010, 200503, ISSN 0031-9007.

Wallentowitz, S. & Vogel, W. (1996). Unbalanced homodyning for quantum state measurements. *Phys. Rev. A*, Vol. 53, No. 6, June 1996, 4528–4533, ISSN 1050-2947.

Zambra, G.; Bondani, M.; Spinelli, A. S.; Paleari, F., & Andreoni, A. (2004). Counting photoelectrons in the response of a photomultiplier tube to single picosecond light pulses. *Rev. Sci. Instrum.*, Vol. 75, No. 8, August 2004, 2762–2765, ISSN 0034-6748 print/1089-7623 online.

Zambra, G.; Andreoni, A.; Bondani, M.; Gramegna, M.; Genovese, M; Brida, G.; Rossi, A., & Paris, M. G. A. (2005). Experimental reconstruction of photon statistics without photoncounting. *Phys. Rev. Lett.*, Vol. 95, No. 6, August 2005, 063602, ISSN 0031-9007.

Zambra, G.; Allevi, A.; Andreoni, A.; Bondani, M., & Paris, M. G. A. (2007). Nontrivial photon statistics with low resolution-threshold photon counters. *Int. J. Quant. Inf.*, Vol. 5, No. 1-2, February-April 2007, 305–309, ISSN 0219-7499.

Zavatta, A.; Viciani, S., & Bellini, M. (2006). Non-classical field characterization by high-frequency, time-domain quantum homodyne tomography. *Laser Phys. Lett.*, Vol. 3, No. 1, January 2006, 3–16, ISSN 1612-2011print/1612-202X online.

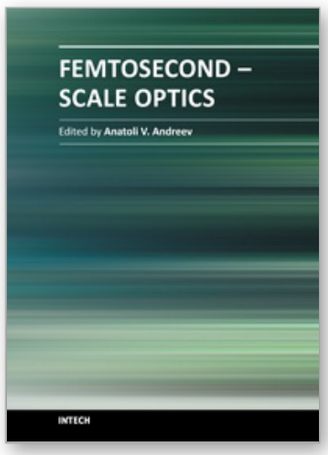

Femtosecond-Scale Optics
Edited by Prof. Anatoly Andreev

ISBN 978-953-307-769-7
Hard cover, 434 pages
Publisher InTech
Published online 14, November, 2011
Published in print edition November, 2011

With progress in ultrashort ultraintense laser technologies the peak power of a laser pulse increases year by year. These new instruments accessible to a large community of researchers revolutionized experiments in nonlinear optics because when laser pulse intensity exceeds or even approaches intra-atomic field strength the new physical picture of light-matter interaction appears. Laser radiation is efficiently transformed into fluxes of charged or neutral particles and the very wide band of electromagnetic emission (from THz up to x-rays) is observed. The traditional phenomena of nonlinear optics as harmonic generation, self-focusing, ionization, etc, demonstrate the drastically different dependency on the laser pulse intensity in contrast the well known rules. This field of researches is in rapid progress now. The presented papers provide a description of recent developments and original results obtained by authors in some specific areas of this very wide scientific field. We hope that the Volume will be of interest for those specialized in the subject of laser-matter interactions.

INTECH
open science | open minds

InTech Europe
University Campus STeP Ri
Slavka Krautzeka 83/A
51000 Rijeka, Croatia
Phone: +385 (51) 770 447
Fax: +385 (51) 686 166
www.intechopen.com

InTech China
Unit 405, Office Block, Hotel Equatorial Shanghai
No.65, Yan An Road (West), Shanghai, 200040, China
中国上海市延安西路65号上海国际贵都大饭店办公楼405单元
Phone: +86-21-62489820
Fax: +86-21-62489821

IntechOpen